Segregated *versus* Mixed Interchain Stacking in Highly Oriented Films of Naphthalene Diimide Bithiophene Copolymers

Martin Brinkmann,[†,*] Eric Gonthier,[†] Stéfan Bogen,[†] Kim Tremel,[‡] Sabine Ludwigs,[‡] Martin Hufnagel,[§] and Michael Sommer[⊥,§]

[†]Institut Charles Sadron, CNRS—Université de Strasbourg, 23 rue du loess, 67034 Strasbourg, France, [‡]Institute für Polymerchemie, Pfaffenwaldring 55, 70569 Stuttgart, Germany, and [§]Melville Laboratory for Polymer Synthesis, Lensfield Road, Cambridge CB2 1EW, U.K. [⊥]Present address: Institut für Makromolekulare Chemie, Universität Freiburg, Stefan-Meier-Straße 31, 79104 Freiburg, Germany

ABSTRACT Highly oriented films of an electron accepting polymer semiconductor, poly{[*N*,*N*′-bis(2-octyldodecyl)-1,4,5,8-naphthalene-dicarboximide-2,6-diyl]-alt-5,5′-(2,2′-bithiophene)} (PNDI2OD-T2), are obtained by two different methods, namely directional epitaxial crystallization (DEC) on 1,3,5-trichlorobenzene (TCB) and epitaxy on friction transferred poly(tetrafluoroethylene) (PTFE) substrates. Two distinct polymorphs with unprecedented intrachain resolution are identified by high-resolution transmission electron microscopy (HR-TEM). Form I is obtained by DEC on TCB, whereas highly oriented films of form II are obtained on PTFE substrates after melting at $T = 300$ °C and cooling at 0.5 K/min. In form I, both electron diffraction and HR-TEM indicate a segregated stacking of bithiophene (T2) and naphthalene diimide (NDI) units forming separate columns. In form II, a ∼c/2 shift between successive π-stacked chains leads to mixed π-overlaps of T2 and NDI. Form I can be transformed into form II by annealing at $T > 250$ °C. The different π-stacking of NDI and T2 in the two polymorphs have characteristic signatures in the UV−vis spectra, especially in the charge transfer band around 750 nm which is also observed in spin-coated films.

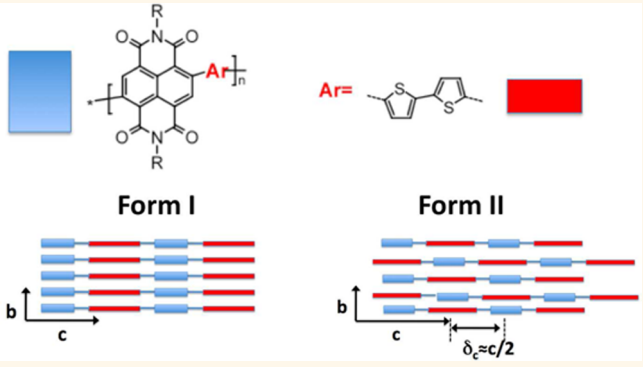

KEYWORDS: naphthalene diimide copolymers · semiconducting polymers · orientation · epitaxy · polymorphism

Control of structure formation and nanomorphology in thin active layers of organic electronic devices is an essential step toward their rational optimization.[1,2] Whereas initial benchmarks of efficient devices were achieved with homogeneous polymers such as poly(3-hexylthiophene) (P3HT),[3−5] small bandgap polymers with alternating electron-rich and electron-poor aromatic units are now established in high-mobility ambipolar organic field effect transistors (OFETs) and very efficient organic photovoltaics (OPVs).[6−14] The heterogeneity of the conjugated backbone with alternating donor and acceptor units provides additional possibilities of interchain interactions. Many small bandgap polymers show a low degree of long-range order yet exhibit strong $\pi-\pi$ interactions in thin films, and hence little is known about the precise stacking mode and the way it impacts the optical and electronic properties in thin films.[15−19] Small band gap polymers based on diketo-pyrrolo-pyrrole or thienopyrrole have recently been reported to exhibit a lamellar structure and significant crystallinity.[20,21] In the case of poly(cyclopentadithiophene-*alt*-benzothiadiazole), Tsao *et al.* demonstrated that intrachain segregation results in short interchain donor−donor and acceptor−acceptor contacts.[22] Rylene diimide copolymers with alternating naphthalene diimide (NDI) or perylene diimide (PDI) and electron-rich comonomers are a promising class of new materials that has been investigated only recently.[23−29] In particular, poly{[*N*,*N*′-bis(2-octyldodecyl)-1,4,5,8-naphthalenedicarboximide-2,6-diyl]-alt-5,5′-(2,2′-bithiophene)} (see Figure 1a),

* Address correspondence to martin.brinkmann@ics-cnrs.unistra.fr.

Received for review September 12, 2012 and accepted October 23, 2012.

Published online October 23, 2012
10.1021/nn304213h

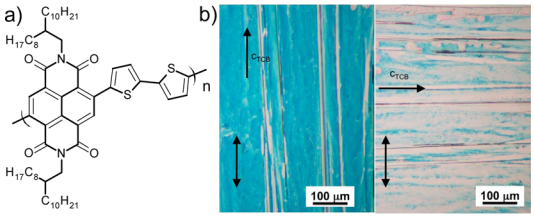

Figure 1. (a) Chemical structure of P(NDI2OD-T2); (b) polarized optical microscopy image of a highly oriented P(NDI2OD-T2) thin film grown by directional epitaxial crystallization on TCB (see text). The upper arrows indicate the direction of TCB crystallization, and the lower ones indicate the orientation of the incident light polarization.

P(NDI2OD-T2), has shown excellent electron mobilities under ambient conditions while being relatively insensitive to processing conditions and molecular weight.[25,26] Moreover, OPV devices based on blends of P(NDI2OD-T2) and P3HT have reached promising efficiencies up to 1.4%.[29] At the same time, the morphology, the preferred orientation, and the semicrystalline microstructure of P(NDI2OD-T2) have attracted much interest, and correlations between thermal treatments, charge mobility, and optical absorption of thin films have been established.[30−32] The choice of the solvent also influences UV−vis absorption in solution.[29] However, in spite of considerable progress, it is not yet clear how P(NDI2OD-T2) chains are packed in a crystalline lattice,[30] and how this packing impacts the overall electronic and optical properties in the solid state, especially in thin films.

The present work addresses the important question of the stacking of T2 and NDI units in the crystalline phases of P(NDI2OD-T2). To this aim, highly oriented and crystalline thin films were prepared by both epitaxy on oriented polytetrafluoroethylene (PTFE) thin films and also by directional epitaxial crystallization (DEC) in 1,3,5-trichlorobenzene (TCB). The former method uses the high orienting ability of friction-transferred PTFE substrates[33] combined with proper thermal annealing protocols. The latter, DEC, is another very powerful epitaxial orientation method that makes use of the crystallizable solvent TCB. TCB plays two roles: in the molten state ($T > 63$ °C), TCB is a solvent for the polymer. Upon cooling ($T < 63$ °C) TCB forms large platelet-shaped domains playing the role of a substrate for epitaxy of the conjugated polymer upon directional crystallization in a temperature gradient.[34−36] In the present report, two different preparation methods result in two different crystalline forms as identified by high-resolution transmission electron microscopy (HR-TEM) and electron diffraction (ED). Most strikingly, HR-TEM enables the direct observation of the two crystal structures corresponding to segregated (form I) and mixed stacks (form II) of P(NDI2OD-T2) chains with unprecedented intrachain resolution, which in turn can be correlated with distinct changes in the absorption spectra.

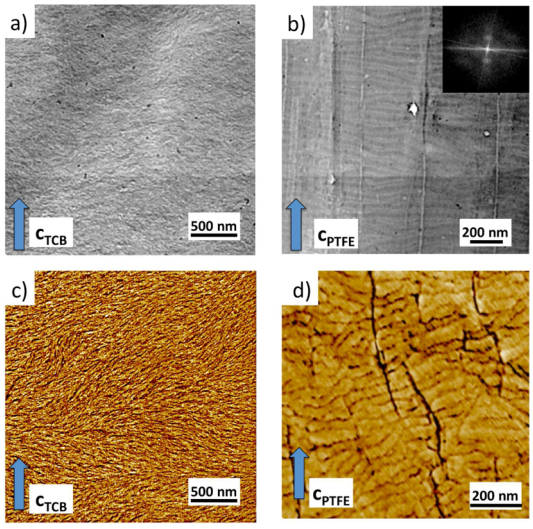

Figure 2. Comparison of the thin film morphologies in bright-field and AFM for P(NDI2OD-T2) thin films grown by directional epitaxial crystallization on 1,3,5-trichlorobenzene (TCB) (a,c) and epitaxy on oriented PTFE (b,d).

RESULTS AND DISCUSSION

Epitaxy is an elegant method to grow highly oriented and crystalline films of conjugated polymers. Here we use two methods to orient P(NDI2OD-T2): alignment layers of PTFE and directional epitaxial crystallization (DEC). As an example, Figure 1 shows the polarized optical microscopy (POM) image of an oriented P(NDI2OD-T2) thin film grown by slow DEC following the improved growth protocol described by Hartmann *et al.*[37]

The two types of oriented P(NDI2OD-T2) films show clear morphology differences, as seen in the TEM bright field mode (BF) (Figure 2a,b) and phase mode AFM images (Figure 2c,d). The morphology of P(NDI2OD-T2) films grown by DEC can only be observed upon strong defocusing in BF. It consists of nanofibrilar structures and is similar to earlier reports for spin-coated thin films.[30−32] In strong contrast, P(NDI2OD-T2) films oriented on PTFE show a periodic and very regular lamellar morphology (Figure 2b,d). The lamellae are oriented essentially perpendicular to the PTFE fibers. In regions without PTFE fibers, no extended lamellar growth is observed, which highlights the nucleating and orienting character of the PTFE substrate. The high crystallinity of these films is at variance with earlier reports of essentially amorphous films after thermal annealing at 300 °C and quenching to room temperature.[32] This difference underlines both, (i) the intrinsic difficulty of nucleation of P(NDI2OD-T2) from the melt which is presently overcome by the use of a nucleating substrate of PTFE and (ii) the necessity to cool P(NDI2OD-T2) films very slowly to allow for efficient crystallization. The regularity of the lamellar structure observed on PTFE is further reflected in the fast Fourier transform (FFT) of the BF image (see inset in Figure 2b),

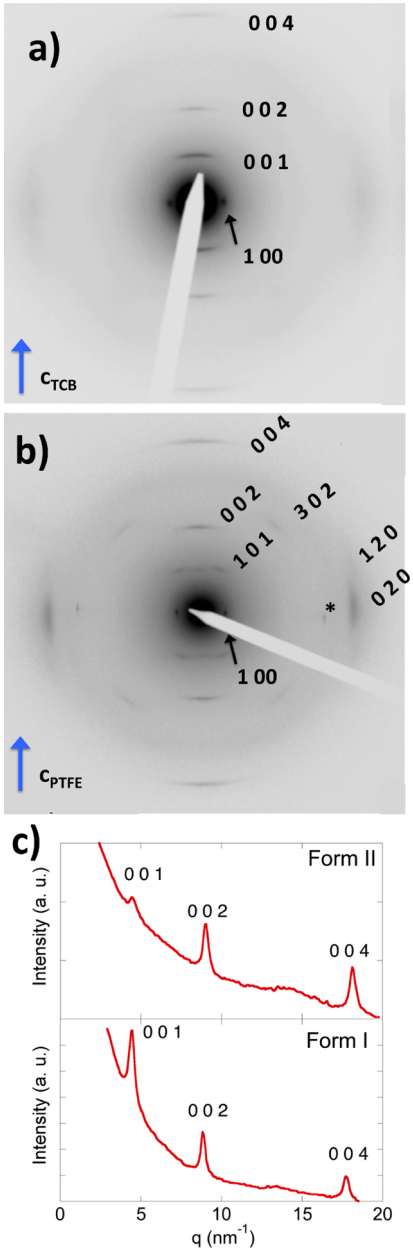

Figure 3. Comparison of the ED patterns of oriented P(NDI2OD-T2) thin films grown on 1,3,5-trichlorobenzene (TCB) by directional epitaxial crystallization (a) and on oriented PTFE (b). (c) Cross-section profile along the meridian of the ED patterns showing the relative intensities of the (00l) reflections. The star in panel b denotes the 100 reflection of the PTFE substrate.

which indicates a lamellar periodicity of 55 ± 5 nm. This lamellar morphology is reminiscent of the ribbon-phase of poly(2,5-bis(3-alkylthiophen-2-yl)thieno[3,2-b]-thiophene) (PBTTT),[38,39] and the extended-chain lamellae of oriented polyfluorene films.[36,40] Attempts to visualize the film morphology by dark field imaging were not successful because the observed reflections in the diffraction patterns were too weak, which in turn translates into a weak contrast in the BF images. The origin of the weak contrast in the BF image is presumably different from that of P3ATs that form

TABLE 1. Reticular Distances Obtained from Electron Diffraction of Oriented Thin Films of P(NDI2OD-T2) Grown under Form I and II[a]

structure *h k l*	form II d_{hkl} (Å)	form I d_{hkl} (Å)
1 0 0	24.7	24.95
2 0 0	12.37	
$(1\ 0\ 0)_{PTFE}$ *	4.9 *	
0 2 0	4.0	3.96
0 0 1	14.1	13.97
1 0 1	12.85	
0 0 2	7.1	7.01
3 0 2	5.33	
0 0 4	3.56	3.51

[a] The reflection marked by an asterisk is a reference corresponding to the (100) reflection of PTFE.

alternating crystalline and amorphous zones.[34] One possible origin of this weak contrast may arise from a difference in film morphology and/or thickness, such as the formation of a factory-roof morphology with alternating thicker and thinner zones, which was observed for polyfluorene.[36] At this point, it appears that owing to the higher chain rigidity of P(NDI2OD-T2) and the relatively low degree of polymerization, chain folding likely does not occur. The lamellar morphology is further confirmed by AFM in the phase mode (Figure 2d). As for polyfluorenes, the lamellae are separated by narrow boundaries. The ribbon thickness has a broad distribution, while the edges of the ribbons are well-defined and straight. This suggests extended-chain crystallization and possibly reflects the polydispersity of the sample. To estimate the degree of polymerization DP_w and the corresponding contour length l_c, we used a combination of SEC calibration[41] and ^{1}H NMR end group analysis (see Supporting Information, Figures S1 and S2). We estimated an DP_w = 34 and l_c = 47 nm. This is in good agreement with the lamellar thickness of 55 nm obtained from TEM, and the typical ribbon average thicknesses of 51 ± 8 nm from AFM. Hence, a scenario of extended chains that are oriented perpendicular to the ribbons and have their chain ends between them is probable.

Electron diffraction (ED) was further used to address the origin of the different morphologies of oriented films grown on TCB and PTFE. Figure 3 shows the ED patterns of the two highly oriented P(NDI2OD-T2) thin films grown by DEC on TCB (Figure 3a) and by epitaxy on an alignment layer of PTFE (Figure 3b). The d_{hkl} values of the reflections are collected in Table 1. Indexation was made using unit cell axes oriented in a similar way as for P3HT, namely **a**, **b** and **c** are along the side chain direction, the π-stacking direction and along the conjugated backbone, respectively. Regarding the ED of the TCB-oriented films, it consists essentially of a sequence of 00l reflections along the meridian and a rather sharp 100 reflection corresponding to the distance between stacks of conjugated backbones separated by

layers of alkyl side chains. The absence of a strong 020 reflection on the equator indicates that the crystalline domains show preferential face-on orientation (Figure 3a). In contrast, the ED pattern of P(NDI2OD-T2) thin films crystallized on PTFE is better defined and shows mixed-indices reflections, pointing at a higher overall crystallinity as compared to the TCB-oriented films. On the equator, both a sharp 100 and a broad and intense 020 reflection are observed, pointing at the coexistence of face-on and edge-on oriented domains (Figure 3b).

The ED patterns of the two type of films do not only differ in terms of preferential orientations of the crystalline domains, but also a remarkable difference is observed when the intensities of the meridional reflections are compared. In both patterns, a set of well-defined meridional reflections corresponding to a period along the chain direction of 1.4 $\pm$ 0.1 nm is observed. This period matches the length of one repeat unit NDI-T2, as obtained from a molecular model of the monomer NDI-T2 in which the two thiophene rings are in the trans conformation, and is nearly identical for the films grown on PTFE and by DEC. This suggests that the chain conformation is similar in both types of structures. Although the ED patterns of the DEC and PTFE films indicate similar reticular distances, the relative intensities of the 00l (l = 1−4) reflections differ significantly. To visualize this more clearly, Figure 3c depicts the section profiles of the ED patterns along the meridian. For the films grown on TCB, the intensity sequence is $I_{001} > I_{002} \approx I_{004}$, whereas for PTFE films it is $I_{001} < I_{002} \approx I_{004}$. Since the monomer repeat period is preserved, the different intensities of the 00l reflections evidence a different mode of π-stacking of the chains in both types of films. The quasi-absence of the 001 reflection for the films grown on PTFE indicates unambiguously that the unit cell of the structure contains two chains with a relative shift of approximately $c/2$ along the chain direction. In contrast, the strong 001 reflection for the TCB-oriented films indicates that the NDI and T2 units in the chains are stacked in a segregated way. Accordingly, ED demonstrates clearly the existence of two polymorphs, confirming previous indications by Rivnay *et al.*[30] We will refer to form I for the TCB-oriented films and form II for the PTFE-oriented films.

To further corroborate the finding of two different stacking modes of NDI and T2 units resulting in form I and II, we calculated the fiber diffraction patterns for the two polymorphs (Supporting Information, Figure S4). To simplify the structural modeling, the branched 2-octyldodecyl side chain was replaced by a linear *all trans* dodecyl side chain oriented perpendicular to the conjugated backbone. Following DFT calculations by Schuettfort *et al.*,[32] a torsional angle of 46° between the T2 and the NDI unit was introduced. The unit cell was chosen so as to contain two nonequivalent chains as obtained by using, somewhat arbitrarily, a $P\bar{1}$ space

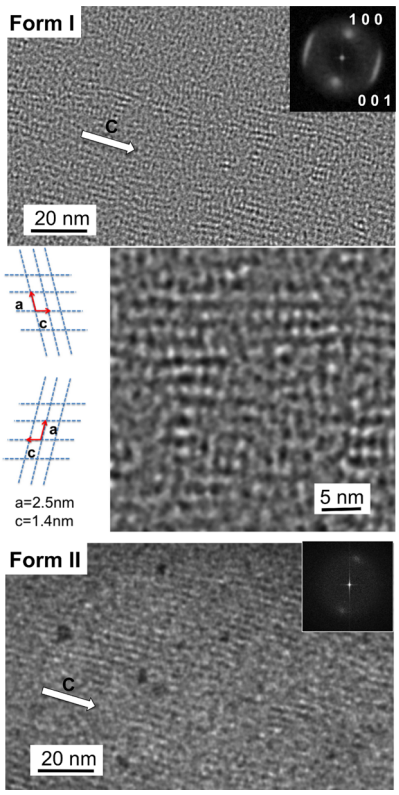

Figure 4. HR-TEM of oriented thin films of P(NDI2OD-T2). Form I is obtained by directional epitaxial crystallization on TCB. Form II is obtained by epitaxy on oriented PTFE substrates after annealing at 300 °C and cooling at 0.5 K/min to ambient temperature. The insets correspond to the fast Fourier transforms of the HR-TEM images. A schematic showing a twinning of the unit cell of form I is also shown.

group. The **b** parameter of the cell was therefore set to 0.8 nm, which is twice the observed π-stacking distance. Models were constructed so as to minimize interchain interatomic short contacts. Figure S4 of the Supporting Information shows the calculated fiber patterns for the totally segregated and the mixed stacking of NDI and BT units. The two structural models reproduce very well the relative intensities of the meridonal 00l reflections. As inferred from our TEM results, the model obtained for form I does show a strong, albeit incomplete, overlap of NDI units of π-stacked chains. In contrast to this, form II shows a strong π-overlap of NDI and T2 units owing to a $c/2$ shift between stacked chains that explains the predominance of the 002 over the 001 reflection. Importantly, different models with branched and without alkyl side chains yielded similar features; that is, the relative intensities of the 00l reflections in the calculated fiber patterns follow the same trend as a function of the relative shift between the two chains in the unit cell.

Attempts were made to visualize the two different stacking modes of NDI and T2 units using high-resolution TEM. The use of HR-TEM was possible because both films show "face-on" oriented domains with layers of π-stacked conjugated chains separated

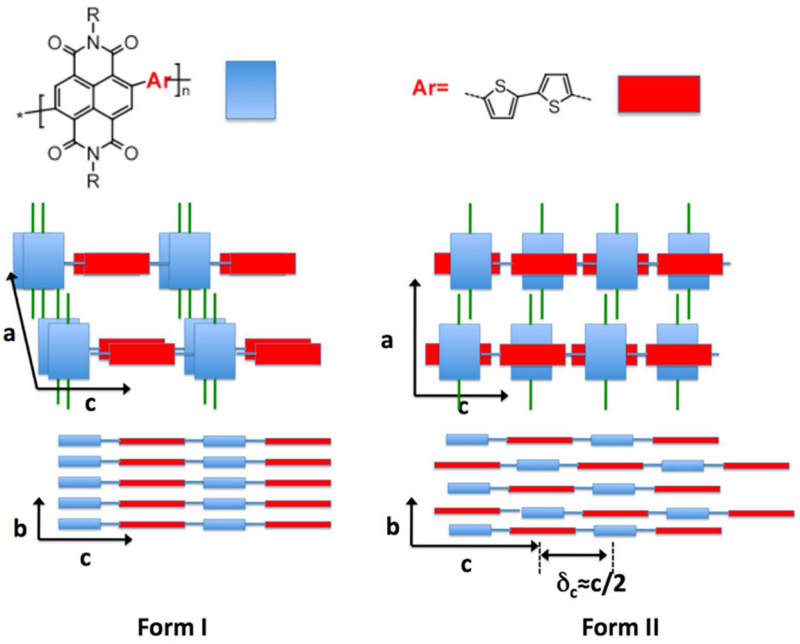

Figure 5. Schematic illustration of the stacking of NDI and T2 units for form I and II of P(NDI2OD-T2). In form I, NDI and T2 units are forming segregated columns which leads to a predominant 001 meridional reflection in the ED pattern. In form II, NDI and T2 units are in π-overlap one with another, leading to dominant meridional 002 due to a *c*/2 shift between the two chains and a very weak 001.

by layers of alkyl side chains.[42,43] As demonstrated in our earlier work on P3HT, the contrast in the HR-TEM image stems from the presence of sulfur in the backbone.[42] In the case of P(NDI2OD-T2), beside the contrast expected between the conjugated backbone containing sulfur atoms and the layers of alkyl side chains, one may potentially observe a *Z* contrast along the chain direction because P(NDI2OD-T2) is made of an alternation of sufur-containing T2 and sulfur-free NDI units. To observe this intrachain *Z*-contrast, T2 and NDI units must form separate columns oriented along the film normal (see Figure 5). Figure 4 shows HR-TEM images of the oriented P(NDI2OD-T2) films grown by DEC in TCB and by epitaxy on PTFE substrates. For both films, one can observe a fringed pattern as observed for face-on oriented P3HT crystallites.[42] The periodicity of the patterns is 2.5 nm; it corresponds to alternating layers of π-stacked P(NDI2OD-T2) backbones and layers of 2-octyldodecyl side chains (**a**-direction). Nevertheless, for films grown on TCB, the HR-TEM images reveal an additional 1.4 nm periodic pattern along the chain axis direction (*c*-direction). In the case of P(NDI2OD-T2), sulfur is present only in T2 moieties and therefore, a single chain shows a characteristic Z contrast modulation along the chain axis. To observe such a periodicity in a thin film involving several layers of P(NDI2OD-T2), all T2 units must stack one on top of another in a direction parallel to the incident electron beam. In other words, the HR-TEM image of P(NDI2OD-T2) films oriented on TCB shows a periodic Z contrast modulation that corresponds to alternating columns of T2 and NDI units, both being oriented along the normal of the film plane. This result is in perfect agreement with the corresponding electron diffraction (ED) pattern of form I showing an intense 001 reflection (Figure 3). Importantly, both the ED and FFT of the HR-TEM image show the same features: an arced 001 reflection and a sharp 100 reflection. A closer inspection of the HR-TEM images further suggests a monoclinic unit cell for form I that exhibits a specific twinning as illustrated schematically in Figure 4.

The structure of P(NDI2OD-T2) films oriented on PTFE is different. Despite repeated attempts, no modulation of the *Z* contrast along the chain axis direction could be detected by HR-TEM. The HR-TEM images show only the fringed pattern corresponding to layers of π-stacked P(NDI2OD-T2) chains separated by layers of 2-octyldodecyl side chains. Hence, HR-TEM further confirms the results of ED, demonstrating that the packing of the P(NDI2OD-T2) chains is different for the films grown on PTFE. Accordingly, this structure does not lead to pure T2 and NDI stacks but to a mixed stacking mode, that is, a different crystal packing referred to as form II. A similar mixed stacking was also observed in F8BT films after annealing of the thin films above the melting temperature.[44] Interestingly, the observed stem length in the direction of the chain axis exceeds 50 nm which is much larger than the average stem length in crystalline P3HT lamellae observed by HR-TEM (it exceeds hardly 20 nm in epitaxied thin films).[37,42,43] This observation confirms the higher rigidity of P(NDI2OD-T2) chains and the extended-chain crystallization mode. The two different types of packing of form I and form II are schematically depicted in Figure 5.

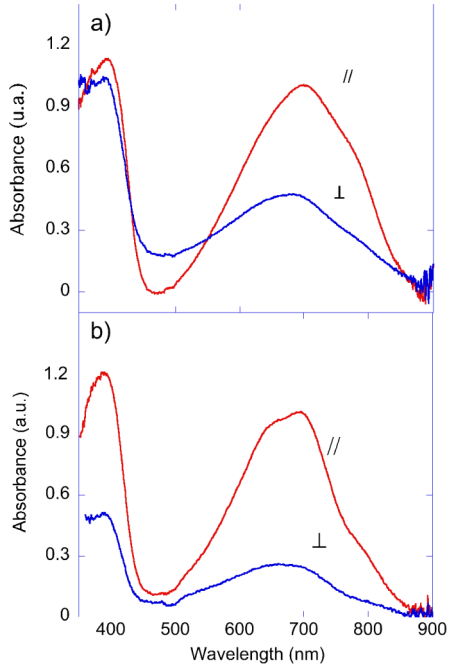

Figure 6. Polarized UV−vis absorption spectra of highly oriented P(NDI2OD-T2) thin films oriented by DEC on TCB (a) and epitaxy on alignment layers of PTFE (b). In the case of PTFE, the films were annealed at 300 °C for 1 min and subsequently cooled at 0.5 K/min to room temperature.

Finally, the different stacking modes of P(NDI2OD-T2) chains in the TCB- and PTFE-oriented films were further characterized by UV−vis spectroscopy. The polarized UV−vis absorption spectra of both oriented P(NDI2OD-T2) films are shown in Figure 6. As expected for two different stacking modes, the spectra of the two films differ significantly in the low energy region of the spectra around 810 nm. Form I is characterized by a broad and structured absorption band centered at 700 nm (dichroic ratio in the range 2−2.5) with a second vibronic band at 810 nm. By contrast, in form II, the absorption band at 810 nm appears as a very weak shoulder, whereas two bands centered at 656 and 692 nm are prominent (dichroic ratio at 693 nm in the range 4−5). The high energy band of form I at 393 nm is almost unpolarized, whereas for form II the band at 389 nm is strongly polarized.

As a general rule, small bandgap polymers exhibit two main absorption bands of high and low energy, which are assigned to $\pi-\pi^*$ excitation and intrachain charge transfer (CT) excitation.[45,46] Here, the important differences in the absorption spectra of form I and form II suggest that the interchain packing influences the structure of the CT and $\pi-\pi^*$ bands presumably *via* interchain excitonic coupling. In particular, the 810 nm band may be assigned to the presence of segregated stacks of NDI and T2 units in P(NDI2OD-T2) thin films. Here, as indicated by the evolution of the UV−vis absorption spectra (see Supporting Information, Figure S5), form I obtained from DEC on TCB can be transformed into form II after annealing the films at $T > 250$ °C. Although the DSC melting temperature of P(NDI2OD-T2) is 300.6 °C (see Supporting Information, Figure S3), annealing at $T > 250$ °C is sufficient to disrupt the segregated π-stacking of NDI and T2 units and to induce a mixed π-stacking. Accordingly, form I may correspond to a kinetically trapped structure made possible by the very strong $\pi-\pi$ interactions between NDI units, while form II could be the thermodynamically more stable form in which steric repulsion of side chains is minimized. Intrachain dipoles that are present in P(NDI2OD-T2) may also contribute to the different driving forces that govern structure formation, which will be the topic of further investigations.[44] In the perspective of photovoltaic applications, mastering absorption in the low energy range ($\lambda > 700$ nm) is essential to improve the light harvesting capability of the active layers. Another result of this study therefore indicates that controlling the growth of a given polymorphic form enables fine-tuning the optical properties of the films in the visible to NIR region.

CONCLUSIONS

Highly oriented films of two polymorphs of P(NDI2OD-T2) were prepared by directional epitaxial crystallization (DEC) on TCB and epitaxy on PTFE substrates. Structural and morphological features of the two polymorphs have been investigated by AFM, electron diffraction, and low-dose high-resolution TEM. The unit cells of the two polymorphs, which differ in terms of stacking of T2 and NDI units, have been identified. To our knowledge, this is the first direct observation of intrachain segregation in a small bandgap conjugated polymer using low-dose HR-TEM. The determination of the polymorphism of P(NDI2OD-T2) can thus help to clarify the emerging debate about correlations between chain stacking and the corresponding optical and charge transport properties in thin films,[47,48] which may finally be useful for other small band gap conjugated polymers with high performance as well.[6−14]

METHODS

P(NDI2OD-T2) was synthesized and purified according to Watson *et al.*[49] except that 5,5′-bis(trimethylstannyl)-2,2′-bithiophene was used. The P(NDI2OD-T2) sample had a number average molecular weight of 21.8 kg/mol and a polydispersity of 3.82, as obtained from SEC against polystyrene calibration. These values were calibrated[41] and combined with informations from ^{1}H NMR end group analysis, from which a degree of polymerization $DP_w = 34$ and a contour length $l_c = 47$ nm was estimated. The detailed procedure can be followed in the Supporting Information.

PTFE substrates were prepared according to the method described elsewhere[50] by sliding a PTFE rod at a constant pressure (5 bar) against a clean glass slide (Corning 2947) held

at 250−300 °C. Thin films of P(NDI2OD-T2) were prepared by doctor-blading a 4 wt % solution in chloroform on the PTFE substrates maintained at 45 °C. The thickness of the films determined by AFM was in the range 30−100 nm. Annealing was performed by using a THMS-600 hot stage (Linkam) connected to a TMS-94 temperature controller. Prior to annealing under nitrogen, the chamber of the hot stage was purged several times with nitrogen. Typical thermal cycles involved melting above 300 °C for 1 min followed by slow cooling to room temperature at 0.5 K/min.

The preparation of oriented films by DEC in TCB was performed using a protocol described by Hartmann *et al.*[37] A mixture of 0.5 wt % P(NDI2OD-T2) in TCB was molten and solidified to prepare a uniform powder. A 25 mg portion of this powder was sandwiched between a PTFE-coated slide and a PEDOT:PSS-coated glass slide. After the first melting and crystallization, a local zone melting was performed using the setup described in reference 13. The molten zone formed a 2 mm wide stripe. This zone was moved at 40 μm/s to perform directional crystallization of TCB and thus epitaxial crystallization of P(NDI2OD-T2). TCB was evaporated at room temperature at 10^{-2} mbar leaving a highly oriented P(NDI2OD-T2) film on the PEDOT:PSS-coated glass substrate. Figure 1 shows such an oriented P(NDI2OD-T2) film observed by polarized optical microscopy.

For TEM observations, the P(NDI2OD-T2) films were coated with a thin layer of amorphous carbon. For PTFE substrates, the carbon-coated film was removed from the glass substrate using aqueous HF solution (5 wt %). In the case of DEC, the films were simply floated onto water. The layers were subsequently picked up using TEM copper grids. TEM was performed in bright-field, high-resolution mode and electron diffraction configurations on a CM12 Philips microscope equipped with a MVIII CCD camera (Soft Imaging Systems). The detailed low-dose method to obtain HR-TEM images is described in reference 42.

The surface topography of the thin films was investigated by atomic force microscopy (AFM) with a Nanoscope III in tapping mode using Si tips (25−50 N/m and 280−365 kHz). Image treatments (FFT) were performed by using AnalySIS (Soft Imaging System) and SXM (NIH) softwares. UV−vis−near IR absorption spectra of the thin films (300−900 nm) were obtained on a Shimadzu UV-2101PC spectrometer with polarized incident light and 1 nm spectral resolution. Structural models and calculated fiber patterns were generated using the appropriate modules of the Cerius2 software (Accelrys).

Conflict of Interest: The authors declare no competing financial interest.

Acknowledgment. Dr. Bernard Lotz is gratefully acknowledged for his help in the composition of this manuscript. The authors are also grateful to Martin Heeney, Imperial College London, for providing the T2 monomer, and to Hartmut Komber, IPF Dresden, for carrying out ^{1}H NMR end group analysis. Financial support from the EU (Interreg Rhin-Solar project) is gratefully acknowledged. M.S. acknowledges funding from the EPSRC. Financial support from the IRTG SoMaS is gratefully acknowledged.

Supporting Information Available: Size exclusion chromoatography; ^{1}H NMR spectra; differential scanning calorimetry data; calculated electron diffraction patterns and corresponding packing models; UV−vis spectra of oriented films after annealing. This material is available free of charge *via* the Internet at http://pubs.acs.org.

REFERENCES AND NOTES

1. James, D. I., Smith, J., Heeney, M., Anthopoulos, T. D., Salleo, A. ; McCulloch, I. *Organic Semiconductor Materials for Transistors, in Organic Electronics II: More Materials and Applications*, Wiley-VCH Verlag: Weinheim. Germany, 2012; pp 1−155.
2. Forrest, S. R. The Path to Ubiquitous and Low-Cost Organic Electronic Appliances on Plastic. *Nature* **2004**, *428*, 911–918.
3. Sirringhaus, H.; Brown, P. J.; Friend, R. H.; Nielsen, M. M.; Bechgaard, K.; Langeveld-Voss, B. M. W.; Spiering, A. J. H.; Janssen, R. A. J.; Meijer, E. W.; Herwig, P.; *et al.* Two-dimensional Charge Transport in Self-Organized, High-Mobility Conjugated Polymers. *Nature* **1999**, *401*, 685–688.
4. Ma, W.; Yang, C.; Gong, X.; Lee, K.; Heeger, A. J. Thermally Stable, Efficient Polymer Solar Cells with Nanoscale Control of the Interpenetrating Network Morphology. *Adv. Funct. Mater.* **2005**, *15*, 1617–1622.
5. McCulloch, I.; Heeney, M.; Bailey, C.; Genevicius, K.; MacDonald, I.; Shkunov, M.; Sparrowe, D.; Tierney, S.; Wagner, R.; Zhang, W.; *et al.* Liquid-Crystalline Semiconducting Polymers with High Charge-Carrier Mobility. *Nat. Mater.* **2006**, *5*, 328–333.
6. Beaujuge, P. M.; Fréchet, J. M. J. Molecular Design and Ordering Effects in π-Functional Materials for Transistor and Solar Cell Applications. *J. Am. Chem. Soc.* **2011**, *133*, 20009–20029.
7. Liang, Y.; Yu, L. A New Class of Semiconducting Polymers for Bulk Heterojunction Solar Cells with Exceptionally High Performance. *Acc. Chem. Res.* **2010**, *43*, 1227–1236.
8. Wang, E.; Hou, L.; Wang, Z.; Hellström, S.; Zhang, F.; Inganäs, O.; Andersson, M. R. An Easily Synthesized Blue Polymer for High-Performance Polymer Solar Cells. *Adv. Mater.* **2010**, *22*, 5240–5244.
9. Sonar, P.; Singh, S. P.; Li, Y.; Siang Soh, M.; Dodabalapur, A. A Low-Bandgap Diketopyrrolopyrrole-Benzothiadiazole-Based Copolymer for High-Mobility Ambipolar Organic Thin-Film Transistors. *Adv. Mater.* **2010**, *22*, 5409–5413.
10. Chen, Z.; Lee, M. J.; Ashraf, R. S.; Gu, Y.; Albert-Seifried, S.; Nielsen, M. M.; Schroeder, B.; Anthopoulos, T. D.; Heeney, M.; McCulloch, I.; *et al.* High-Performance Ambipolar Diketopyrrolopyrrole-Thieno[3,2-*b*]thiophene Copolymer Field-Effect Transistors with Balanced Hole and Electron Mobilities. *Adv. Mater.* **2012**, *24*, 647–652.
11. Kronemeijer, A. J.; Gili, E.; Shahid, M.; Rivnay, J.; Salleo, A.; Heeney, M.; Sirringhaus, H. A Selenophene-Based Low-Bandgap Donor−Acceptor Polymer Leading to Fast Ambipolar Logic. *Adv. Mater.* **2012**, *24*, 1558–1565.
12. Fan, J.; Yuen, J. D.; Wang, M.; Seifter, J.; Seo, J.-H.; Mohebbi, A. R.; Zakhidov, D.; Heeger, A.; Wudl, F. High-Performance Ambipolar Transistors and Inverters from an Ultralow Bandgap Polymer. *Adv. Mater.* **2012**, *24*, 2186–2190.
13. Bijleveld, J. C.; Zoombelt, A. P.; Mathijssen, S. G. J.; Wienk, M. M.; Turbiez, M.; de Leeuw, D. M.; Janssen, R. A. J. Poly(diketopyrrolopyrrole-terthiophene) for Ambipolar Logic and Photovoltaics. *J. Am. Chem. Soc.* **2009**, *131*, 16616–16617.
14. Li, W.; Roelofs, W. S. C.; Wienk, M. M.; Janssen, R. A. J. Enhancing the Photocurrent in Diketopyrrolopyrrole-Based Polymer Solar Cells *via* Energy Level Control. *J. Am. Chem. Soc.* **2012**, *134*, 13787–13795.
15. Zhang, M.; Tsao, H. N.; Pisula, W.; Yang, C.; Mishra, A. K.; Müllen, K. Field-Effect Transistors Based on a Benzothiadiazole−Cyclopentadithiophene Copolymer. *J. Am. Chem. Soc.* **2007**, *129*, 3472–3473.
16. Guo, J.; Liang, Y.; Szarko, J.; Lee, B.; Jung Son, H.; Rolczynski, B. S.; Yu, L.; Chen, L. X. Structure, Dynamics, and Power Conversion Efficiency Correlations in a New Low Bandgap Polymer: PCBM Solar Cell. *J. Phys. Chem. B* **2010**, *114*, 742–748.
17. Zhang, W.; Smith, J.; Watkins, S. E.; Gysel, R.; McGehee, M.; Salleo, A.; Kirkpatrick, J.; Ashraf, S.; Anthopoulos, T.; Heeney, M.; McCulloch, I. Indacenodithiophene Semiconducting Polymers for High-Performance, Air-Stable Transistors. *J. Am. Chem. Soc.* **2010**, *132*, 11437–11439.
18. Yiu, A. T.; Beaujuge, P. M.; Lee, O. P.; Woo, C. H.; Toney, M. F.; Fréchet, J. M. J. Side-Chain Tunability of Furan-Containing Low-Band-Gap Polymers Provides Control of Structural Order in Efficient Solar Cells. *J. Am. Chem. Soc.* **2012**, *134*, 2180–2185.
19. Piliego, C.; Holcombe, T. W.; Douglas, J. D.; Woo, C. H.; Beaujuge, P. M.; Fréchet, J. M. J. Synthetic Control of Structural Order in *N*-Alkylthieno[3,4-*c*]pyrrole-4,6-dione-Based Polymers for Efficient Solar Cells. *J. Am. Chem. Soc.* **2010**, *132*, 7595–7597.

20. Zhang, X.; Richter, L. J.; DeLongchamp, D. M.; Kline, R. J.; Hammond, M. R.; McCulloch, I.; Heeney, M.; Ashraf, R. S.; Smith, J. N.; Anthopoulos, T. D.; *et al.* Molecular Packing of High-Mobility Diketo Pyrrolo-Pyrrole Polymer Semiconductors with Branched Alkyl Side Chains. *J. Am. Chem. Soc.* **2011**, *133*, 15073–15084.
21. Guo, X.; Ortiz, R. P.; Zheng, Y.; Kim, M.-G.; Zhang, S.; Hu, Y.; Lu, G.; Facchetti, A.; Marks, T. J. Thieno[3,4-*c*]pyrrole-4,6-dione-Based Polymer Semiconductors: Toward High-Performance, Air-Stable Organic Thin-Film Transistors. *J. Am. Chem. Soc.* **2011**, *133*, 13685–13697.
22. Tsao, H. N.; Cho, D. M.; Park, I.; Hansen, M. R.; Mavrinskiy, A.; Yoon, D. Y.; Graf, R.; Pisula, W.; Spiess, H. W.; Müllen, K. Ultrahigh Mobility in Polymer Field-Effect Transistors by Design. *J. Am. Chem. Soc.* **2011**, *133*, 2605–2612.
23. Zhan, X.; Tan, Z.; Domercq, B.; An, Z.; Zhang, X.; Barlow, S.; Li, Y.; Zhu, D.; Kippelen, B.; Marder, S. R. A High-Mobility Electron-Transport Polymer with Broad Absorption and Its Use in Field-Effect Transistors and All-Polymer Solar Cells. *J. Am. Chem. Soc.* **2007**, *129*, 7246–7247.
24. Chen, Z.; Zheng, Y.; Yan, H.; Facchetti, A. Naphthalenedicarboximide- *vs* Perylenedicarboximide-Based Copolymers. Synthesis and Semiconducting Properties in Bottom-Gate N-Channel Organic Transistors. *J. Am. Chem. Soc.* **2009**, *131*, 8–9.
25. Yan, H.; Chen, Z.; Zheng, Y.; Newmann, C.; Quinn, J. R.; Dötz, F.; Kastler, M.; Facchetti, A. A High-Mobility Electron-Transporting Polymer for Printed Transistors. *Nature* **2009**, *457*, 679–686.
26. Guo, X.; Sunjoo Kim, F.; Seger, M. J.; Jenekhe, S. A.; Watson., M. D. Naphthalene Diimide-Based Polymer Semiconductors: Synthesis, Structure−Property Correlations, and *n*-Channel and Ambipolar Field-Effect Transistors. *Chem. Mater.* **2012**, *24*, 1434–1442.
27. Zhou, E.; Cong, J.; Zhao, M.; Zhang, L.; Hashimoto, K.; Tajima, K. Synthesis and Application of Poly(fluorene-*alt*-naphthalene diimide) as an n-Type Polymer for All-Polymer Solar Cells. *Chem. Commun.* **2012**, *48*, 5283–5285.
28. Zhou, E. J.; Cong, J. Z.; Wei, Q. S.; Tajima, K.; Yang, C. H.; Hashimoto, K. All-Polymer Solar Cells from Perylene Diimide Based Copolymers: Material Design and Phase Separation Control. *Angew. Chem., Int. Ed.* **2011**, *50*, 2799–2803.
29. Schubert, M.; Dolfen, D.; Frisch, J.; Roland, S.; Steyrleuthner, R.; Stiller, B.; Chen, Z.; Scherf, U.; Koch, N.; Facchetti, A.; *et al.* Influence of Aggregation on the Performance of All-Polymer Solar Cells Containing Low-Bandgap Naphthalenediimide Copolymers. *Adv. Energy Mater.* **2012**, *2*, 369–380.
30. Rivnay, J.; Toney, M. F.; Zheng, Y.; Kauvar, I. V.; Chen, Z.; Wagner, V.; Facchetti, A.; Salleo, A. Unconventional Face-On Texture and Exceptional In-Plane Order of a High Mobility n-Type Polymer. *Adv. Mater.* **2010**, *22*, 4359–4363.
31. Rivnay, J.; Steyrleuthner, R.; Jimison, L. H.; Casadei, A.; Chen, Z.; Toney, M. F.; Facchetti, A.; Neher, D.; Salleo, A. Drastic Control of Texture in a High Performance n-Type Polymeric Semiconductor and Implications for Charge Transport. *Macromolecules* **2011**, *44*, 5246–5255.
32. Schuettfort, T.; Huettner, S.; Lilliu, S.; Macdonald, J. E.; Thomsen, L.; McNeill, C. R. Surface and Bulk Structural Characterization of a High-Mobility Electron-Transporting Polymer. *Macromolecules* **2011**, *44*, 1530–1539.
33. Wittmann, J.-C.; Smith, P. Highly Oriented Thin Films of Poly(tetrafluoroethylene) as a Substrate for Oriented Growth of Materials. *Nature* **1991**, *352*, 414–417.
34. Brinkmann, M.; Wittmann, J.-C. Orientation of Regioregular Poly(3-hexylthiophene) by Directional Solidification: A Simple Method to Reveal the Semicrystalline Structure of a Conjugated Polymer. *Adv. Mater.* **2006**, *18*, 860–863.
35. Brinkmann, M.; Rannou, P. Effect of Molecular Weight on the Structure and Morphology of Oriented Thin Films of Regioregular Poly(3-hexylthiophene) Grown by Directional Epitaxial Solidification. *Adv. Funct. Mater.* **2007**, *17*, 101–108.
36. Brinkmann, M. Directional Epitaxial Crystallization and Tentative Crystal Structure of Poly(9,9′-di-*n*-octyl-2,7-fluorene). *Macromolecules* **2007**, *40*, 7532–7541.
37. Hartmann, L.; Tremel, K.; Uttiya, S.; Crossland, E.; Ludwigs, S.; Kayunkid, N.; Vergnat, C.; Brinkmann, M. 2D *versus* 3D Crystalline Order in Thin Films of Regioregular Poly-(3-hexylthiophene) Oriented by Mechanical Rubbing and Epitaxy. *Adv. Funct. Mater.* **2011**, *21*, 4047–4057.
38. Jung Lee, M.; Gupta, D.; Zhao, N.; Heeney, M.; McCulloch, I.; Sirringhaus, H. Anisotropy of Charge Transport in a Uniaxially Aligned and Chain-Extended, High-Mobility, Conjugated Polymer Semiconductor. *Adv. Funct. Mater.* **2011**, *21*, 932–940.
39. Delongchamp, D. M.; Kline, R. J.; Jung, Y.; Germack, D. S.; Lin, E. K.; Moad, A. J.; Richter, L. J.; Toney, M. F.; Heeney, M.; McCullouch, I. Controlling the Orientation of Terraced Nanoscale "Ribbons" of a Poly(thiophene) Semiconductor. *ACS Nano* **2009**, *3*, 780–787.
40. Brinkmann, M.; Charoenthai, N.; Traiphol, R.; Piyakulawat, P.; Wlosnewski, J.; Asawapirom, U. Structure and Morphology in Highly Oriented Films of Poly(9,9-bis(*n*-octyl)fluorene-2,7-diyl) and Poly(9,9-bis(2-ethylhexyl)fluorene-2,7-diyl) Grown on Friction Transferred Poly(tetrafluoroethylene). *Macromolecules* **2009**, *42*, 8298–8306.
41. Senkovskyy, V.; Tkachov, R.; Komber, H.; John, A.; Sommer, J.-U.; Kiriy, A. Mechanistic Insight into Catalyst-Transfer Polymerization of Unusual Anion-Radical Naphthalene Diimide Monomers: An Observation of Ni(0) Intermediates. *Macromolecules* **2012**, *45*, 7770–7777.
42. Brinkmann, M.; Rannou, P. Molecular Weight Dependence of Chain Packing and Semicrystalline Structure in Oriented Films of Regioregular Poly(3-hexylthiophene) Revealed by High-Resolution Transmission Electron Microscopy. *Macromolecules* **2009**, *42*, 1125–1130.
43. Salammal, T. S.; Mikayelyan, E.; Grigorian, S.; Pietsch, U.; Koenen, N.; Scherf, U.; Kayunkid, N.; Brinkmann, M. Impact of Thermal Annealing on the Semicrystalline Nanomorphology of Spin-Coated Thin Films of Regioregular Poly-(3-alkylthiophene)s as Observed by High-Resolution Transmission Electron Microscopy and Grazing Incidence X-ray Diffraction. *Macromolecules* **2012**, *45*, 5575–5585.
44. Donley, C. L.; Zaumseil, J.; Andreasen, J. W.; Nielsen, M. M.; Sirringhaus, H.; Friend, R. H.; Kim, J.-S. Effects of Packing Structure on the Optoelectronic and Charge Transport Properties in Poly(9,9-di-*n*-octylfluorene-*alt*-benzothiadiazole). *J. Am. Chem. Soc.* **2005**, *127*, 12890–12899.
45. Jespersen, K. G.; Beenken, W. J. D.; Zaushitsyn, Y.; Yartsev, A.; Andersson, M.; Pullerits, T.; Sundström, V. The Electronic States of Polyfluorene Copolymers with Alternating Donor−Acceptor Units. *J. Chem. Phys.* **2004**, *121*, 12613–12617.
46. Winfield, J. M.; Van Vooren, A.; Park, M.-J.; Hwang, D. H.; Cornil, J.; Kim, J. S.; Friend, R. H. Charge-transfer character of excitons in poly[2,7-(9,9-di-*n*-octylfluorene)$_{(1-x)}$-*co*-4,7-(2,1,3-benzothiadiazole)$_{(x)}$]. *J. Chem. Phys.* **2009**, *131*, 035104.
47. Fazzi, D.; Caironi, M.; Castiglioni, C. Quantum-Chemical Insights into the Prediction of Charge Transport Parameters for a Naphthalenetetracarboxydiimide-Based Copolymer with Enhanced Electron Mobility. *J. Am. Chem. Soc.* **2011**, *133*, 19056–19059.
48. Surin, M.; Sonar, P.; Grimsdale, A. C.; Müllen, K.; Lazzaroni, R.; Leclerc, P. Supramolecular Organization in Fluorene/Indenofluorene− Oligothiophene Alternating Conjugated Copolymers. *Adv. Funct. Mater.* **2005**, *15*, 1426–1434.
49. Guo, X .; Watson, M. D. Conjugated Polymers from Naphthalene Bisimide. *Org. Lett.* **2008**, *10*, 5333–5336.
50. Brinkmann, M.; Graff, S.; Wittmann, J.-C.; Chaumont, C.; Nuesch, F.; Anver, A.; Schaer, M.; Zuppiroli, L. Orienting Tetracene and Pentacene Thin Films onto Friction-Transferred Poly(tetrafluoroethylene) Substrate. *J. Phys. Chem. B* **2003**, *107*, 10531–10539.